



Extended summary

Study of nanostructured materials by electron microscopy and X-ray diffraction techniques

Curriculum: Materials, Waters and Soils Engineering

Author

Eleonora Santecchia

Tutors

Prof. Paolo Mengucci

Prof. Erio Pasqualini

Date: 30-01-2014

Abstract. This work deals with the application of electron microscopy and X-ray diffraction techniques to the structural characterisation of innovative nanostructured materials of possible use in materials science. Based on the characteristics of each specific material analysed, three main different applicative fields have been addressed: a) materials for solid state hydrogen storage (thin films and nanocomposites), b) materials for biomedical applications (biomaterials and detectors), and c) light metal alloys for automotive and aeronautical applications.

Keywords. Electron microscopy, Energy dispersive microanalysis, Nanostructured materials, Structural characterization, X-ray diffraction.



Doctoral School on Engineering Sciences

Università Politecnica delle Marche

1 Problem statement and objectives

The structural characterization of nanomaterials is the crucial step in the scientific research on the nanomaterials applications, because it allows to “observe” what really happens inside the material, giving to the researchers the possibility of correlating the results to the physical and chemical properties of the analysed samples.

In the present work several characterization techniques based on X-ray diffraction and electron microscopy were applied: X-ray diffraction (XRD), scanning electron microscopy (SEM), transmission electron microscopy (TEM) and energy dispersive spectroscopy (EDS). All these techniques have been used to characterize materials mainly produced for the following applications:

- Solid state hydrogen storage;
- Biomedical devices and prosthesis;
- Light metal alloys for automotive and aeronautics.

Aim of this work was, therefore, to prepare and characterize materials with different physical and chemical properties in order to correlate their microstructural features to the macroscopic behaviour required by each specific application the single nanomaterials were designed for.

In particular, for the solid-state hydrogen storage nanomaterials the attention was focused on the structural modifications induced by the repeated H₂ absorption/desorption cycles under which the samples were submitted. In this case, possible correlations between the structural modifications and the hydrogen storage capacity of the material were discussed.

On the contrary, in the field of biomaterials and light alloys the microstructural modifications of the materials studied mainly accounted for the variation of their mechanical behaviour.

2 Research planning and activities

The work on samples addressing all the different above cited applications was carried out simultaneously. After sample preparation, tensile tests, light yield measurements, hydrogenation cycles, microhardness tests and other types of measurements have been performed on the samples, according to their specific applicative fields. Afterwards, structural characterization has been performed by means of:

- X-ray diffraction (XRD) measurements;
- scanning electron microscopy (SEM) observations;
- transmission electron microscopy (TEM) observations;
- energy dispersive spectroscopy (EDS) microanalysis.

Two kinds of materials for solid state hydrogen storage have been examined: Mg-based thin films and Pd-PDMS composites.

The thin films were deposited by r.f. magnetron sputtering and Mg was chosen as the main element because of its ability to store a high amount of hydrogen (7.6 wt.%).



Despite the excellent capacity of hydrogen storage, pure magnesium has slow reaction kinetics; to overcome this drawback, Mg thin films doped with 5at.% of a transition metal (Nb) were deposited. All the films were coated with a Pd cap layer (20 nm) to protect them from oxidation and to facilitate the dissociation of hydrogen on the surface.

The samples were subjected to several cycles of H₂ absorption/desorption and samples subjected to 1, 2, 4, and 8 cycles, as well as those in the as-deposited condition (reference) were then subjected to the structural characterization.

Even after the Nb addition, samples still suffered from structural issues such as the de-crepitation (i.e. effective pulverization of the films due to the interaction hydrogen). To overcome this issues, literature [1] suggested to synthesize composite materials. Therefore, composite samples made of Pd and PDMS (polysilicon, Saratoga formulation) were prepared and subjected to hydrogenation cycles and structural characterization.

In the field of materials for biomedical applications, metal alloys for dental and orthopaedic implants and scintillating crystals as detectors for PET, have been studied. In the first case, the attention has been focused on a CoCrMo alloy produced by a rapid prototyping technique such as Direct Metal Laser Sintering (DMLS). The structural characterization was performed on samples subjected to mechanical tests in order to correlate the mechanical properties to the microstructure. The mechanical properties and light yield of four LYSO:Ce scintillating crystals have been related to their structural features.

Light metal alloys for aeronautical purposes have been also investigated: two well known alloys, AZ31B Mg alloy and 2219 aluminum alloy, were subjected to two different treatments: the AZ31B alloy was welded by friction stir welding (FSW), while the AA2219 alloy was subjected to Equal Channel Angular Pressing (ECAP). The microstructure of the alloys was studied by electron microscopy techniques, in order to correlate the effects of the two procedures on the microstructures of the considered light alloys.

3 Analysis and discussion of the main results

3.1 Materials for solid state hydrogen storage

Magnesium-based alloys have attracted a lot of attention thanks to the high storage capacity of H₂ and at low cost: pure Mg can store up to 7.6 wt% H₂ [2].

Two kinds of thin films have been studied:

- pure Mg films (Mg-Nb 0at.%);
- Nb-doped Mg (Mg-Nb 5at.%).

The thin films have a thickness of about 30 μm and have been deposited by r.f. magnetron sputtering on graphite in Ar atmosphere [3]. After deposition, the samples were peeled off the graphite substrate. The self supporting samples were then introduced in a volumetric apparatus for H₂ cycling and for studying the isothermal sorption kinetics at 350°C [3-5]. The results are reported in Figure 1, where is clear that reactions kinetics are an order of magnitude faster in the case of the Nb-doped samples.

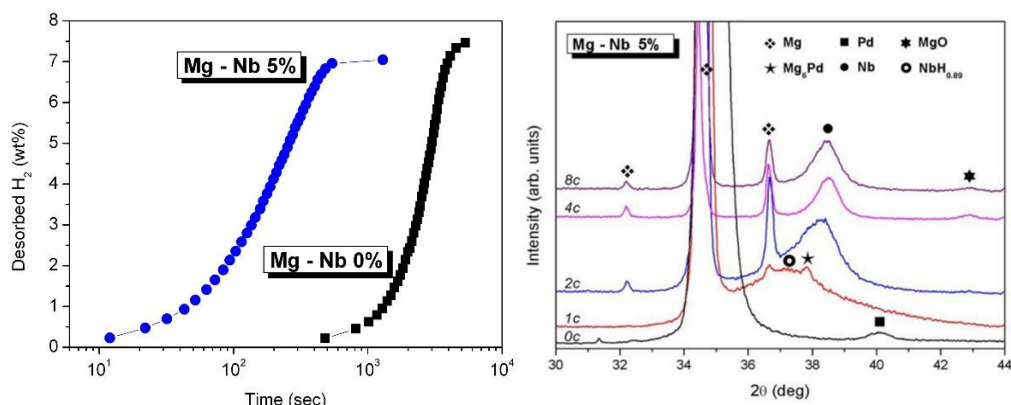


Figure 1. Reaction kinetics of the pure Mg and Nb-doped thin films (*left*). XRD spectra of the Nb-doped thin films (*right*).

On the right side of Figure 1 the results of the XRD measurements on the Nb-doped samples are reported. The deconvolution of the NbH_{0.89} (200) and to the Nb (100) reflections, gave an average dimension of the Nb particles of about 10 nm, obtained by applying the Scherrer formula [6,7].

The composite samples were obtained by dispersing different amounts of Pd particles in a polydimethylsiloxane (PDMS) matrix. Polysiloxane belongs to a class of polymeric materials available on the market that exhibit high permeation rates to hydrogen even at room temperature [8].

The metallic fraction is the commercially available palladium black powder provided by Sigma-Aldrich (99,9% Pd), used without fractioning for the preparation of the composite material.

Three different compositions were prepared with a nominal Pd content (in wt%) of:

- 5% (sample A);
- 15% (sample B);
- 50% (sample C).

Pd is the only element that absorbs hydrogen at ambient temperature and pressure forming an interstitial metallic hydride PdH_{0.67} [9].

Hydrogen storage capacity and desorption kinetics of samples with different Pd content were analyzed in a Sievert type apparatus [10]. According to the US DOE goal for hydrogen storage to be reached until 2015 (working temperature in the range between -40 °C and +80 °C) [11], investigations at different temperatures (60°C, 80°C and 100°C) and operational pressures (from 0,2 atm to 2 atm) were carried out, in order to obtain a complete characterization of the sample kinetics [12].

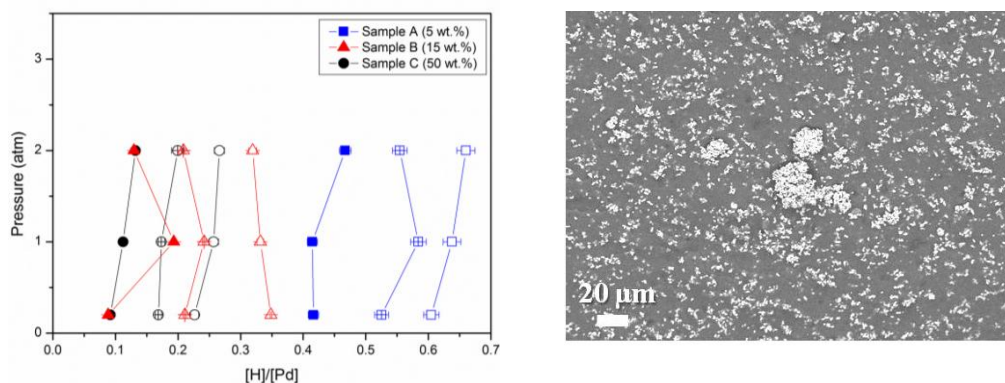


Figure 2. Left: Hydrogen storage performance of the composites. The horizontal axis of the figure reports the H content with respect to the composite metal fraction. Solid symbol - 60 °C, open crossed symbol - 80 °C and open symbol - 100 °C. Left: SEM micrograph of sample C (50 % Pd).

The SEM micrograph reported in Figure 2 (right) evidences the tendency of the metal particles to aggregates. The size of these metal clusters increases with the amount of the metallic fraction, reaching a maximum for sample C (Pd 50%). This effect is mainly attributable to the large dimensions of the powder particles, which could not imply any nanoconfinement effect [1].

From the graph reported on the left side of Figure 2, the influence of the temperature and absorption pressure values on the hydrogen storage properties of the composites is evident. The hydrogen stored amount increases with temperature for all compositions while the absorption pressure value, at constant composition and temperature, has a limited influence on it. On the contrary, the content of the metallic fraction in the composite material seems to play an important role. In fact, sample A (Pd 5%) stores a higher hydrogen amount (about 3-4 times) than samples B (15 wt.%) and C (50 wt.%). This latter effect could be related to the mean size of the metallic clusters formed in the composite materials at the different concentrations.

3.2 Materials for biomedical applications

3.2.1 Biomaterials: CoCrMo biocompatible alloy produced by DMLS

Additive manufacture of metallic parts is assuming a rising importance and generally involves the consolidation of metal powder particles via a focused energy source in the form of either a laser or an electron beam [13].

Direct metal laser sintering (DMLS) is an AM process using the heat of a solid state laser to sinter metal powder particles. In particular, a distribution mechanism is used to pre-place successive powder layers, which are locally sintered or melted in accordance with the CAD model [14]. A scanning system controls the laser movements across the powder bed. This technology, as other AM procedures, is highly rewarding in medicine, where a high degree of personalization is required. Prosthetic applications are particularly well-suited for processing by means DMLS due to their complex geometry, low volume and strong individualization [15].

CoCrMo alloys are widely used for biomedical implants such as artificial joints (knees and hips) due to their excellent corrosion resistance, wear resistance and biocompatibility.

Co is characterized by two phases [16]: a γ phase with a face-centered cubic structure (fcc), stable at high temperatures, and a ϵ phase with compact hexagonal structure (hcp), stable at low temperatures. The fcc \rightarrow hcp transformation in Co and its alloys is very slow due to the limited chemical driving forces available to the temperature at which the transformation takes place. Therefore, under normal conditions of cooling, the fcc phase remains within the edge of the phase in the metastable state [16].

X-ray diffraction measurement were performed both on the Co-Cr-Mo powder used as starting material for DMLS process, and on different regions of the sintered samples (Figure 5).

The XRD pattern of the sintered sample in Figure 3 (left) shows simultaneous presence of both γ and ϵ cobalt phases, as indicated in Figure 3 (left) where each diffraction peak is indexed with the name of the corresponding Co phase.

The XRD pattern of the as-received metallic powder, showed only peaks referable to the γ phase: this result indicates that in the analysed samples the laser beam produces a local melting of the metal particles that solidify and cool down quickly due to the thermal conductivity of the alloy, as well as the small heated region. Thus in successive small areas there are conditions very similar to those responsible for the athermal martensitic transformation.

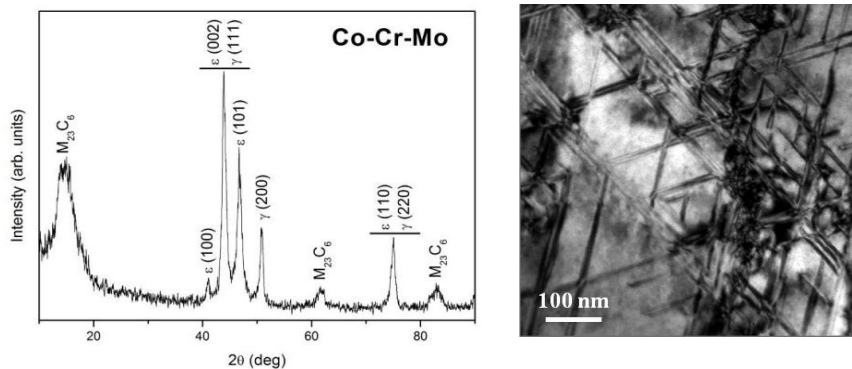


Figure 3. Left: XRD spectrum of the sintered CoCrMo alloy. Right: TEM bright field image of the ϵ lamellae inside the γ phase.

TEM observations (Figure 3 right) of the sintered samples confirm the presence of the two ϵ and γ cobalt phases. The DMLS process on the CoCrMo powder led to the formation of an intricate network of thin ϵ -lamellae inside the γ cobalt phase that was never observed before [17].

3.2.2 Detectors: LYSO:Ce crystals as detectors for Positron Emission Tomography (PET)

The LSO crystals have a combination of excellent properties to be used in PET and for many years have been considered the best material for this kind of detectors [18]. High density, high atomic number, quick decay constant and high emissions of light are some of

their properties. Lutetium gives to this crystals a low level of natural radioactivity such as do not interfere with the signal emitted by the tracers for PET.

The addition of yttrium (Y) and the cerium (Ce) doping, leading to the LYSO:Ce crystals, resulted in a scintillation decay time comparable to LSO, making them promising candidates for applications in medical diagnostics, especially because of the ability to reveal particles of gamma rays of 511 keV.

Four oxorthosilicate crystals of lutetium-yttrium- cerium doped $\text{Lu}_{2(1-x)}\text{Y}_{2x}\text{SiO}_5:\text{Ce}$ with $x = 0.1$ (LYSO), part of the same crystal grown by Czochralski method, have been examined.

Two of the four samples were subjected to an annealing process consists of the following steps: heating ramp of 1 °C/min for 300 minutes, annealing at 300 °C for 10 hours (in air), and air cooling (0.5 °C/min) [19].

Mechanical properties, such as ultimate tensile strength, σ_{UTS} , and Young's modulus, E , were evaluated by performing a four points bending test, generating a constant bending moment on the sample and, consequently, a known distribution of stress in the sample [19]. Results are shown in Table 1.

Table 1. Results of bending test. The samples were numbered according to a criterion established by the manufacturer.

Sample	σ_{UTS} (MPa)	E (MPa)	Annealing
1	94	182	Y
6	68	129	Y
8	78	174	N
10	79	174	N

The samples subjected to annealing (samples 1 and 6) showed the best mechanical properties (sample 1) in terms of σ_{UTS} and E , and the worst overall performance as for sample 6.

The light yield of the four crystals have been measured using the photomultiplier tube with a source of Cesium-137: no remarkable differences have been observed.

The crystals were then crushed in a mortar and subjected to XRD measurements in θ - 2θ configuration ($\theta = 13^\circ$ - 70°) with Cu- $K\alpha$ radiation. The lattice parameters were determined applying the Rietveld refinement method [20] using the FullProf software [21]. The application of the Rietveld method allowed to obtain the space group $I2/a$, compatible with $C2/c$ and the following values of the lattice parameters: $a = 1.421$ nm, $b = 0.661$ nm, $c = 1.024$ nm, and $\beta = 122.11^\circ$. These values of the lattice parameters were confirmed by neutron diffraction measurements.

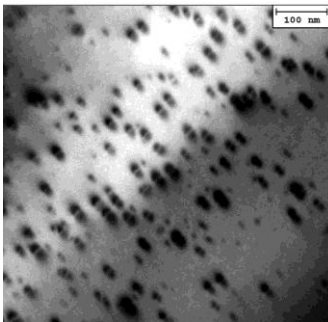


Figure 4. TEM micrograph of sample 6 [22].

TEM observations showed an homogeneous structure for samples 1, 8 and 10. In sample 6, however, TEM revealed the presence of numerous spherical coherent precipitates, contrast with the typical "coffee bean" contrast (Figure 4).

EDS microanalysis performed on the precipitates and on the matrix showed a higher yttrium concentration in the precipitates area.

Sample 6 resulted to be the most interesting due to the presence of coherent precipitates in the microstructure and to its worst mechanical properties, while the other annealed samples (sample 1) showed the best mechanical performance but did not show any particular structural feature.

Therefore, it is likely to suppose that the mechanical properties of the examined LYSO:Ce crystals are influenced by the microstructural characteristics, rather than by the particular annealing treatment.

3.3 Light metal alloys

Light metal alloys are the basics raw materials for industrial and aeronautical applications. Two alloys based on aluminum and magnesium, the well known AA2219 and AZ31B, have been examined. Two different methods of Friction Stir Welding (FSW) have been applied to AZ31B magnesium alloy sheets. The effects of the welding process on the mechanical properties and microstructural joints were investigated by metallographic analysis by light microscopy, Vickers microhardness tests, tensile tests at room temperature and analysis of the fracture zone after tensile tests by means of a scanning electron microscope (SEM) [23].

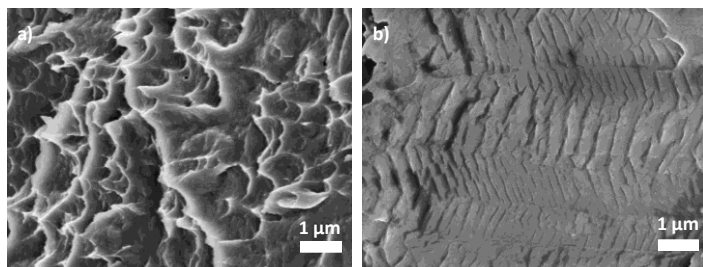


Figure 5. Sample of AZ31B after tensile the test showing : a) dimples, b) cleavage features.

Figure 5 shows the SEM micrographs of the welding after the tensile test: all the samples showed zones with cleavage features and zones with dimples.

The fracture has probably started in the areas of cleavage, then the coalescence of microvoids during application of the load, caused a decrease of the tensile strength and the consequent rupture of the samples. EDS microanalysis performed on the impurities observed in the dimples showed the presence of the elements such as C, Ca and O, confirming their impurities nature, probably due to the FSW process.

The 2219 aluminium alloy has been subjected to equal-channel angular pressing (ECAP) [24] and the strengthening effect of the $(Fe,Mn,Cr)_3Si_2Al_{15}$ intermetallics has been evaluated. Three samples corresponding to the following conditions have been examined:

- as extruded (AE);
- after one ECAP pass through route A (ECAP/A-1);
- after two ECAP passes through route A (ECAP/A-2).

The SEM micrograph of the ECAP/A-2 sample is reported in Figure 6. A stereological method of quantification based on the Woodhead coefficients [25] has been applied to 5 SEM micrographs belonging to each condition, in order to calculate the particle size distribution.

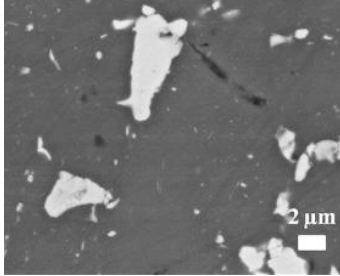


Figure 6. SEM micrograph of the sample after ECAP/A-2 passes.

The quantitative stereological study allowed the calculation of several parameters characterizing the size of the intermetallics and their mutual distances inside the different samples. As reported in literature, the presence of intermetallic compounds contribute to the alloy reinforcement [26]. In order to evaluate the effect of these compounds on the behaviour of the AA2219 alloy, the parameter of intermetallics appearance index (IPA) [27] was calculated, together with the strengthening terms $\Delta\sigma_{LT}$ (fraction of load carried by the intermetallics instead of the matrix) [26] and $\Delta\sigma_{Intermet}$ [28] (alloy strengthening due to the presence of the intermetallics). Table 2 shows the results from the calculations [24,29].

Table 2. Evolution of dimension, volume fraction and the strengthening terms of the $(Fe,Mn,Cr)_3Si_2Al_{15}$ intermetallic particles.

Deformation status	IPA	IPA variation to AE (%)	$\Delta\sigma_{LT}$ (10^{-2} MPa)	$\Delta\sigma_{Intermet}$ (MPa)
AE	$63 \cdot 10^{-3} \pm 0.2$	-	57	1.85
ECAP/A-1	$36 \cdot 10^{-3} \pm 0.4$	44	96	4.4
ECAP/A-2	$32 \cdot 10^{-3} \pm 0.5$	50	88	4.2

*Adapted from [24] and [29].

It is clear from data reported in Table 2 that the values of the IPA and the strengthening terms $\Delta\sigma_{LT}$ and $\Delta\sigma_{Intermet}$ are increased at ECAP/A-1 pass but then remain substantially unchanged at ECAP/A-2 passes. This result fully agrees with literature [26].

All the others contribution to the alloy strengthening have been evaluated from the TEM micrographs. Afterwards, all the microstructure strengthening contributions have been combined as showed by Cabibbo [26] and the result has been compared with the values calculated with the model of the measured proof stress: an extraordinarily “perfect” agreement between experimental and calculated proof stress was obtained in both the ECAP experimental conditions [29].

4 Conclusions

In the present research the structural characterization techniques based on electron microscopy and X-ray diffraction have been applied to several classes of nanostructured materials.

For each class of materials analyzed, the main results can therefore be summarized as follows:

- Nb-doped thin films (Mg-Nb 5%) showed reactions kinetics one order of magnitude faster than those of pure Mg (Mg-Nb 0%): Nb nanoparticles reduce the thermal stability of MgH_2 and accelerate the H_2 desorption kinetics;
- Mg-based thin films becomes porous after the interaction with hydrogen. Moreover Nb particles form clusters enhancing the porous structure formation;
- the Pd-PDMS composite samples showed a particular interaction with hydrogen, placing them in an intermediate position between the bulk structure and the nanoparticles, thus being reasonably considered as structures that have their own scientific identity;
- in the biomedical CoCrMo alloy produced by DMLS, the laser action induces an athermal martensitic phase transformation, producing an intricate network of thin ϵ -lamellae distributed inside the γ phase, never observed before;
- in the LYSO:Ce crystals, sample 6 is the one that shows the worst mechanical properties and is the one whose microstructure is characterized by the presence of spherical coherent precipitates ("coffee bean-like" contrast). The combination of these two effects leads to the conclusion that the microstructural features have a crucial effect on the mechanical properties of the crystals, while the annealing treatment is less important;
- the AZ31B welded by FSW showed a transgranular fracture with cleavage features and dimples, due to the inclusion of impurities during the FSW process;
- the AA2219 subjected to ECAP showed that the intermetallic appearance index (IPA) shows values decreased from the as-extruded to the first ECAP pass, while it remains essentially unchanged with accumulated shear strain. Moreover, the strengthening contribution coming from the intermetallic particles resulted to be an important feature in the calculation of the overall alloy proof stress.

References

- [1] C. Zlotea and M. Latroche. *Role of nanoconfinement on hydrogen sorption properties of metal nanoparticles hybrids*. Colloids and Surfaces A, In press, 2012.
- [2] P. Selvam, B. Viswanathan, C.S. Swamy and V. Srinivasan. *Magnesium and magnesium alloy hydrides*. International Journal of Hydrogen Energy, vol. 11, No. 3, pp. 169–192, 1986.
- [3] R. Checchetto, G. Trettel and A. Miotello. *Sievert-type apparatus for the study of hydrogen storage in solids*. Measurement Science & Technology, vol. 15, No. 1, pp. 127-130, 2004.
- [4] R. Checchetto, N. Bazzanella, A. Miotello and P. Mengucci. *Catalytic properties on the hydrogen desorption process of metallic additives dispersed in the MgH_2 matrix*. Journal of Alloys and Compounds, vol. 446, pp. 58-62, 2007.
- [5] N. Bazzanella, R. Checchetto, A. Miotello, C. Sada, P. Mazzoldi and P. Mengucci. *Hydrogen kinetics in magnesium hydride: On different catalytic effects of niobium*. Applied Physics Letters, vol. 89,



- No. 1, pp. 0141011-0141013, 2006.
- [6] A. Monshi, M.R. Foroughi and M.R. Monshi. *Modified Scherrer equation to estimate more accurately nano-crystallite size using XRD*. World Journal of Nano Science and Engineering, vol. 2, No. 3, pp. 154-160, 2012.
- [7] P. Mengucci, G. Barucca, G. Majni, N. Bazzanella, R. Checchetto and A. Miotello. *Structure modification of Mg-Nb films under hydrogen sorption cycles*. Journal of Alloy and Compounds, vol. 509, No. 2, pp. S572-S575, 2011.
- [8] T.C. Merkel, V.I. Bondar, K. Nagai, B. D. Freeman and I. Pinnau. *Gas sorption, diffusion, and permeation in poly(dimethylsiloxane)*. Journal of Polymer Science Part B: Polymer Physics, vol. 38, No. 3, pp. 415-434, 2000.
- [9] M. Dincă and J.R. Long. *Hydrogen storage in microporous metal-organic frameworks with exposed metal sites*. Angewandte Chemie International Edition, vol. 47, pp. 6766-6779, 2008.
- [10] R. Checchetto, G. Carotenuto, N. Bazzanella and A. Miotello. *Synthesis and characterization of a polymer embedded LaNi₅ composite material for hydrogen storage*. Journal of Physics D, vol. 40, No. 13, pp. 4043-4048, 2007.
- [11] B.D. Adams and A. Chen. *The role of palladium in a hydrogen economy*, Materials Today, vol. 14, No. 6, pp. 282-289, 2011.
- [12] E. Santecchia, G. Barucca, G. Majni, P. Mengucci, R. Checchetto and G. Carotenuto. *Kinetic behaviour of a metal-polymer composite suitable for hydrogen storage applications*. International Journal of Nanotechnology, Accepted, 2014.
- [13] A. Rosochowski and A. Matuszak. *Rapid tooling: the state of the art*. Journal of Materials Processing Technology, vol. 106, No. 1-3, pp. 191-198, 2000.
- [14] E. Bassoli, A. Gatto and L. Iuliano. *Joining mechanisms and mechanical properties of PA composites obtained by Selective Laser Sintering*. Rapid Prototyping Journal, vol. 18, No. 2, pp. 100-108, 2012.
- [15] E. Atzeni, L. Iuliano, P. Minetola and A. Salmi. *Proposal of an innovative benchmark for accuracy evaluation of dental crown manufacturing*. Computers in Biology and Medicine, vol. 42, No. 5, pp. 548-555, 2012.
- [16] H.F. Lopez and A.J. Saldivar-Garcia. *Martensitic transformation in a cast Co-Cr-Mo-C alloy*, Metallurgical and Materials Transactions A, vol. 39, No. 1, pp. 8-18, 2008.
- [17] G. Barucca, E. Santecchia, G. Majni, E. Girardin, E. Bassoli, A. Gatto, L. Iuliano, T. Moskalewicz and P. Mengucci. *Structural characterization of biomedical Co-Cr-Mo components produced by Direct Metal Laser Sintering*, Journal of alloys and Compounds, Submitted, 2014.
- [18] C.L. Melcher and J.S. Schweitzer. *Cerium-doped Lutetium Oxyorthosilicate: A Fast, Efficient New Scintillator*. IEEE Transactions On Nuclear Science, vol. 39, No. 4, pp. 502-505, 1992.
- [19] L. Scalise, D. Rinaldi, F. Davi and N. Paone. *Measurement of ultimate tensile strength and Young modulus in LYSO scintillating crystals*, Nuclear Instruments and Methods in Physics Research A, vol. 654, No. 1, pp. 122-126, 2011.
- [20] H.M. Rietveld. *A Profile Refinement Method for Nuclear and Magnetic Structures*. Journal of Applied Crystallography, vol. 2, No. 2, pp. 65-71, 1969.
- [21] J. Rodriguez-Carvajal. *Recent Developments of the Program FULLPROF*. Commission on Powder Diffraction (IUCr), No. 26, pp. 12-19, 2001.
- [22] E. Auffray, G. Barucca, F. Davi, N. Di Vara, P. Mengucci, L. Montalto, D. Rinaldi and E. Santecchia. *Structural analysis and light yield of LYSO samples*. Manuscript in Preparation.
- [23] G. Quercetti, E. Santecchia, S. Spigarelli, D. Ciccarelli and M. Pieralisi. *Comparazione sui giunti di lega Mg AZ31 saldati FSW da uno e due lati*. La Metallurgia Italiana, vol. 4, pp. 1-9, 2013.
- [24] E. Santecchia, P. Mengucci and M. Cabibbo. *Microstructure and intermetallic strengthening in a Equal Channel Angular Pressed AA2219. Part I: microstructure characterization*. Metallography, Microstructure and Analysis, Submitted in revised version, 2014.
- [25] K.J. Kurzydłowski and B. Ralph. *The quantitative description of the microstructure of materials*. CRC series in Materials Science and Technology, 1995.

- [26] M. Cabibbo. *Microstructure strengthening mechanisms in different equal channel angular pressed aluminum alloys*. Materials Science and Engineering A, vol. 560, pp. 413-432, 2013.
- [27] S.G. Shabestari and M. Ghanbari. *Effect of plastic deformation and semisolid forming on iron-manganese rich intermetallics in Al-8Si-3Cu-4Fe-2Mn alloy*. Journal of Alloys and Compounds, vol. 508, No. 2, pp. 315-319, 2010.
- [28] P.M. Hazledine. *Direct versus indirect dispersion hardening*. Scripta Metallurgica et Materialia, vol. 26, No. 1, pp. 57-58, 1992.
- [29] E. Santecchia and M. Cabibbo. *Microstructure and intermetallic strengthening in a Equal Channel Angular Pressed AA2219. Part II: strengthening model*. Metallography, Microstructure and Analysis, Submitted in revised version, 2014.